agronomy

MDPI

Article

The Impact of Flow Channel Structural Parameters on Both the Hydraulic Performance and Anticlogging Abilities of Variable Flow Emitters

Peining Niu [1,2], Yan Mo [2,*], Baolin Yao [1,*], Zongze Yang [2,3], Yanqun Zhang [2] and Dequan Zhang [4]

[1] College of Water Conservancy and Architectural Engineering, Tarim University, Alaer 843300, China; npn20428@yeah.net
[2] State Key Laboratory of Simulation and Regulation of Water Cycle in River Basin, China Institute of Water Resources and Hydropower Research, Beijing 100048, China; 15135355441@163.com (Z.Y.); zhangyq@iwhr.com (Y.Z.)
[3] College of Water Resources Science and Engineering, Taiyuan University of Technology, Taiyuan 030024, China
[4] Ordos Water Conservancy Development Center, Eerduosi 017000, China; zdq55825669@126.com
* Correspondence: moyan@iwhr.com (Y.M.); 120050078@taru.edu.cn (B.Y.)

Abstract: Variable flow emitters are used in subsurface drip irrigation to address challenges in soil moisture transport. This study investigates the impact of flow channel structural parameters on the hydraulic performance and anticlogging ability of emitters using computational fluid dynamics (CFD) simulations and experimental tests. The results show that the realizable k–ε turbulence model can be used to simulate the flow field inside the variable flow emitter flow channel. The *nRMSE* between the measured (q_m) and simulated (q) values of the flow rate is 11.23%, and the *relative error* between the measured (x_m) and simulated (x) values of the flow index is 4.66%, which gives a high simulation accuracy. A polar analysis shows that the tooth angle (A) has the smallest effect on the effluent flow rate at 0.1 MPa ($q_{0.1}$), x, and particle passage rate (η) of the variable flow emitter. Flow channel depth (D), tooth spacing (B), and tooth height (E) have a different order of precedence in the influence of the three indices, which are D > B > E > A, B > E > D > A and E > B > D > A, respectively. The value of η is positively correlated with the mean flow velocity (v) and the mean turbulent kinetic energy (k) in the flow channel, and η tends to increase and then decrease with the increase of x. The retention time of the particles in the flow channel is closely related to the magnitude of v and k. Three multivariate lin ear regression equations (R^2 = 0.883–0.995) were constructed for $q_{0.1}$, x, and η versus the flow channel structural parameters. The optimal design combination of channel structure parameters for different scenarios was determined using the scipy.optimize.minimize function in Python 3.8.0. The research results provide a reference for the optimal design of variable flow emitters.

Keywords: subsurface drip irrigation; variable flow emitter; flow index; particle passage rate; structure optimization

check for updates

Citation: Niu, P.; Mo, Y.; Yao, B.; Yang, Z.; Zhang, Y.; Zhang, D. The Impact of Flow Channel Structural Parameters on Both the Hydraulic Performance and Anticlogging Abilities of Variable Flow Emitters. *Agronomy* **2024**, *14*, 2560. https://doi.org/10.3390/agronomy14112560

Academic Editors: Pablo Martín-Ramos and Koffi Djaman

Received: 8 August 2024
Revised: 19 September 2024
Accepted: 28 October 2024
Published: 31 October 2024

Copyright: © 2024 by the authors. Licensee MDPI, Basel, Switzerland. This article is an open access article distributed under the terms and conditions of the Creative Commons Attribution (CC BY) license (https://creativecommons.org/licenses/by/4.0/).

1. Introduction

Subsurface drip irrigation (SDI), installed below the soil surface, enhances surface drip irrigation by automating the irrigation process, thus improving efficiency and reducing labor requirements. SDI is the existing irrigation technology with the greatest water–saving potential and is one of the most obvious ways to increase production and improve quality [1–5]. In recent years, SDI has been widely studied in Northwest China [5,6], North China [7,8], and South China [9], but the following problems exist: (1) To avoid soil tillage damage to SDI systems, it is necessary to bury the SDI systems below the soil tillage layer [10]; additionally, the upward transport of soil moisture is less than the downward transport due to gravity [11], which causes delayed crop emergence or nonemergence of seedlings, leading to reduced yields [12–14]. (2) Compared with center pivot sprinklers, SDI systems

must operate for more than 10 years to be economically competitive [15], which implies a substantial increase in the risk of emitter clogging. The enhancement of emitter clogging resistance in SDI systems is critical.

In response to problem (1), Mo et al. [16] proposed a variable flow emitter for SDI that automatically switches the operating phase according to the inlet pressure to achieve a step change in the outlet flow rate. A regular outlet flow rate of 1–2 L/h is provided during working stage I (the regular-flow water supply stage), which is used to supply water to the crop during most of its reproductive period. In work stage II (the high-flow water supply stage), by increasing the water supply pressure, a stepwise increase in the water output flow rate is realized, which promotes the upward movement of soil moisture, improves the soil moisture environment of the seed bed, and thus promotes seedling emergence. Gao et al. [17] took a variable flow emitter as the research object to study its hydraulic performance response law (flow rate and flow index) to the parameters of the channel structure and determined the optimal combination of the channel structure corresponding to the outlet flow rate of 1.5 L/h at 0.1 MPa using a traversal optimization algorithm. However, scholars have neglected the influence of a variable flow emitter channel structure on anticlogging performance.

The hydraulic performance of the emitter determines the uniformity of water and fertilizer application in the whole drip irrigation system [18,19]. The flow rate (q) and flow index (x) are the two main hydraulic performance indices of the emitter, and a smaller x corresponds to a lower sensitivity of the emitter effluent flow rate to the inlet pressure and a greater laying distance [20–22]. Some scholars studying tooth-shaped channel emitters have reported that the channel width, number of cells, channel depth, and tooth height all have significant effects on q [23], the q of tooth-shaped emitters increases with an increasing tooth-turning angle and tooth spacing, tooth width has a greater effect on q than the bottom pitch of the tooth [24,25], and q is positively correlated with the tooth-tip angle and tooth-tip covariance and negatively correlated with the cusp angle and cusp parameter [26,27]. Moreover, most scholars have used hydraulic performance tests and numerical simulations to investigate the primary and secondary order of the influence of the flow channel structural parameters on x. For serrated channel emitters, the primary order is tooth spacing > tooth angle > tooth height > channel depth [28]. The primary order of the structural parameters affecting x changes when the structural parameter takes a different range of values, e.g., tooth base pitch > tooth height > tooth width [29] and channel depth > tooth height > tooth angle > tooth base pitch [30]. For trapezoidal channel emitters, the primary order is channel width > number of channel cells > angle > channel depth [31,32]. For orthogonal labyrinth channels, x is minimized when the intertooth angle is 70° [27].

Reducing q is an important way to increase the length of dripline laying and reduce the investment in drip irrigation systems per unit area [33,34]. Most drip irrigation equipment manufacturers reduce q only by reducing the depth of the flow path, but this drastically increases the risk of emitter clogging. According to a food and agriculture organization, the probabilities of physical, chemical, and biological clogging in the process of emitter clogging are 31%, 22%, and 37%, respectively. Gilbert et al. [35] reported that 55% of emitter clogging is caused by physical factors, with physical clogging caused by solid particles being the most common form [36,37]. Numerous scholars have adopted laser Doppler velocimetry (LDV), particle image velocimetry (PIV), particle tracking velocimetry (PTV), computational fluid dynamics (CFD), and other methods to visualize the operation of particles inside the emitter flow channel and analyze the response laws of the water flow velocity, turbulent kinetic energy in the flow channel, turbulent kinetic energy dissipation rate, and particle passage rate with the structural parameters of the emitter flow channel to increase the ability of the emitter to resist physical clogging. For rectangular and serrated channel emitters, some scholars have applied CFD two-phase flow numerical simulations and PIV technology to analyze the velocity vector, streamline distribution, and particle trajectory of the fluid, pointing out that the tip of the tooth is the most serious region of

turbulent kinetic energy dissipation and the low-speed vortex region at the sharp corners is the focus of the clogging location [38,39]. The clogging resistance of the emitters tends to decrease with increasing channel angles, and the emitters corresponding to a 60° angle were more resistant to clogging [40]. Yu et al. [41,42] used a combination of a CFD–discrete element method (CFD–DEM) coupled numerical simulation and the lattice Boltzmann method with composite weighted average (LS–CWM) laser particle sizer tests to analyze the movement of particles in a flow channel. They proposed that increasing the flow velocity in the low-velocity zone of the flow channel and eddy zone can strengthen the ability of water scouring and sand hostage, reduce the risk of solid particle deposition in the flow channel, and reduce the probability of clogging the emitter. The resistance of toothed channels to clogging was better than that of trapezoidal and triangular channels [43]. For rectangular emitter channels, a channel with an internal tooth width × internal tooth height of 0.8 mm × 0.5 mm has the best clogging resistance [44].

These studies focused on the hydraulic performance and anticlogging performance of the emitter, and few studies have focused on the optimization of the emitter channel structure while comprehensively considering these two properties. Wang [45] constructed a multiobjective optimization model of flow channel parameters, with the objectives of minimizing the steady flow index and maximizing the sediment particle passage rate, using an algorithm that combines non-dominated sorting genetic algorithm II (NSGA-II) and a support vector machine for optimization at a rated flow rate of 3.0 L/h. The flow rate of commonly used emitters in China is typically 1–2 L/h [46,47]. Currently, solving constrained optimization problems using the scipy.optimize.minimize function in Python is both efficient and numerically stable. This function has been widely applied to problems such as risk assessment in emergency decision-making for typhoon disasters [48], benefit distribution in military supply chains [49], and the optimization of overhauling equipment in coal mining enterprises [50]. It is widely regarded as more suitable than other methods for addressing common optimization problems.

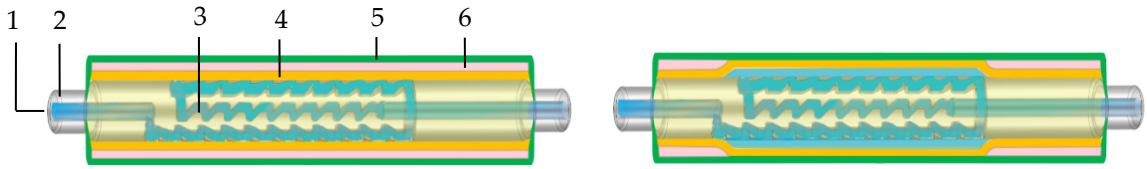
In this study, the variable flow emitter is taken as the research object, with the help of an orthogonal test to set up a tooth-shaped flow channel composed of different tooth heights (E), tooth spacings (B), tooth angles (A), and flow channel depth (D). The sample was precision-machined by computer numerical control (CNC). The hydraulic and anticlogging performance of its working stage I was explored through numerical simulation and indoor tests. In addition, the evaluation indices of its hydraulic and anticlogging performance were constructed with the structure. At the same time, a quantitative characterization mathematical model of hydraulic performance and anticlogging performance evaluation indices and structural parameters were constructed, and the optimized combination of the structural parameters of the variable flow emitter flow channel under different scenarios was obtained using the scipy.optimize.minimize function in Python. The above method overcomes the limitations of traditional irrigator designs, provides an efficient optimization strategy, and offers a reliable theoretical basis and practical guidance for both further research and practical applications.

2. Materials and Methods

2.1. Principle of Operation of a Variable Flow Emitter

When the pressure at the inlet of the variable flow emitter is less than the design step pressure, the water flow can only move in the flow channel of the emitter core, and the variable flow emitter is in the stage of regular-flow water supply, i.e., working stage I, and the water supply flow rate is q_I (Figure 1a). When the inlet pressure is greater than the design step pressure, the pressure of the water flow in the flow channel of the core body makes the elastomer in the cavity formed by the emitter shell and the core body expand and deform, and the elastomer breaks away from the flow channel. When the elastomer is detached from the flow channel, the cross-section of the overflow channel suddenly increases, and the water flow rate from the emitter increases stepwise. This working stage is the high-flow water supply stage, i.e., working stage II, and the water supply flow rate is

q_{II} (Figure 1b). Factors affecting the deformation of the elastomer in stage II mainly include inlet pressure and elastomer mechanical parameters. Variable flow emitters are suitable for subsurface drip irrigation systems [17], with working stage I during most of a crop's reproductive period. They use working stage II during the seedling emergence period to accelerate the upward rate of soil moisture transport by increasing the water flow rate, improving the surface soil moisture environment, and promoting crop emergence.



1. Inlet 2. Core 3. Channel 4. Elastomer 5. Shell 6. Cavity

(**a**) (**b**)

Figure 1. Schematic diagram of the working principle of a variable flow emitter: (**a**) The regular-flow water supply stage; (**b**) The high-flow water supply stage.

In working stage I, the use of smaller flow rate emitters ($q_{0.1}$ < 1.5 L/h) can increase the ultimate laying length of the dripline and reduce the amount of the branch pipe and construction costs, which has received extensive attention from domestic and foreign scholars and drip irrigation equipment manufacturers in recent years. We often reduce $q_{0.1}$ by reducing the size of the flow channel above the water cross-section, but the risk of clogging the emitter increases with the decreasing size of the flow channel [51,52]. Therefore, in this study, performance tests and structural optimization were carried out to test the hydraulic characteristics and clogging resistance of the emitter during the water supply phase at regular flow rates.

2.2. Experimental Design

The variable flow emitter core used in this study consists of three toothed channels (a, c, e) and two curved channels (b, d), with the toothed channels a, c, and e distributed around the axis of the core and connected by curved channels b and d. The water movement direction is left inlet → a → b → c → d → e → right outlet (Figure 2). The total length of the toothed channel is 57.2 mm.

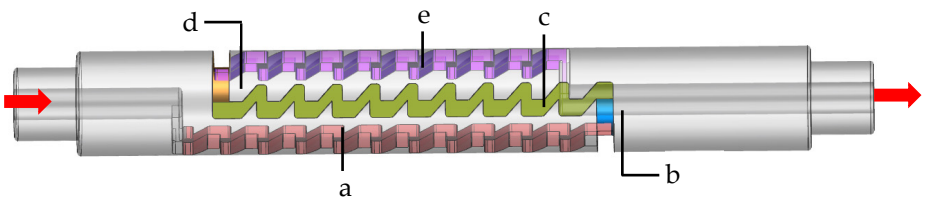
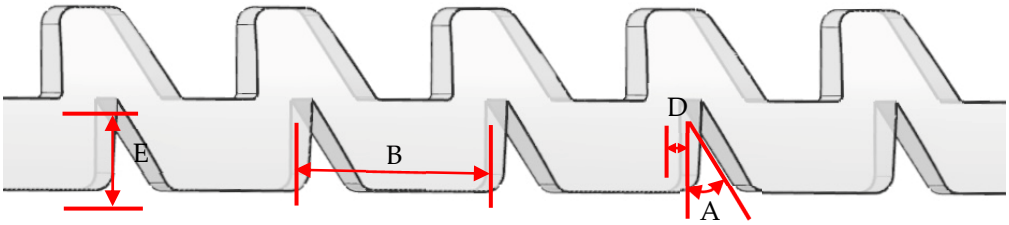


Figure 2. Schematic diagram of the variable-flow emitter channel structure.

The tooth height (E), tooth spacing (B), tooth angle (A), and flow channel depth (D) of the toothed channels were selected for the study (Figure 3). Three levels were set for each parameter, which were designed according to the orthogonal test $L9(3^4)$, totaling nine combinations of channel structure parameters. The variable flow emitter finalized by [17] was added to correct the numerical simulation results with its measured values, which had a $q_{0.1}$ of 1.5 L/h. The experimental design is detailed in Table 1. The total length of the toothed channels was affected mainly by B. To ensure the same total length of the toothed channels when channels a and c were composed of 11 and 10 toothed units, respectively, B had 1.8 mm, 2.0 mm, and 2.2 mm emitters with 9, 6, and 4 toothed units, respectively.



A. Tooth angle B. Tooth spacing D. Flow channel depth E. Tooth height

Figure 3. Schematic diagram of the structural parameters of the toothed channel of the variable flow emitter.

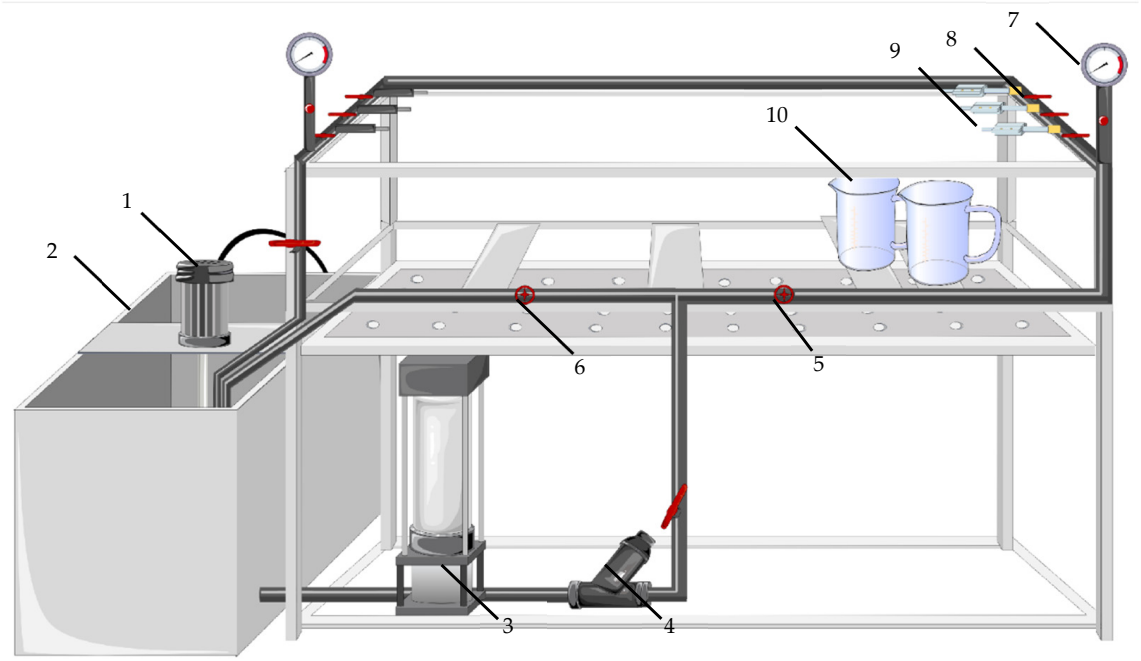
Table 1. Experimental design.

Trial Number	Experimental Factors			
	E/mm	B/mm	A/°	D/mm
1	0.8	1.8	34	0.6
2	0.8	2.0	42	0.8
3	0.8	2.2	38	1.0
4	1.0	1.8	42	1.0
5	1.0	2.0	38	0.6
6	1.0	2.2	34	0.8
7	1.2	1.8	38	0.8
8	1.2	2.0	34	1.0
9	1.2	2.2	42	0.6
10	0.8	1.8	42	0.8

2.3. Hydraulic Performance Tests

The hydraulic performance test experiment of the variable flow emitter was conducted at the China National Water Saving Irrigation Engineering and Technology Research Center (Beijing, Daxing). The test platform is shown in Figure 4. The test water source was local tap water, and the water temperature was maintained at 23 ± 2 °C. The 10# emitter in Table 1 was machined via a precision five-axis CNC machine (with a machining accuracy of 0.002 mm) using 304 stainless steel. The elastomer was chosen because it deforms very little and can form a good sealing polytetrafluoroethylene hard tube (inner diameter of 4.8 mm and outer diameter of 7.8 mm; Taizhou Qingchen Rubber & Plastic Products Co., Ltd., Taizhou, China) to simulate the variable flow emitter in the regular flow of the water supply stage.

The test steps are as follows: The 10# emitter specimen was installed, the valve was closed, and the water receiving container was placed under the emitter. The water pump was turned on (CDLF4 10, flow rate 4 m^3/h, head 0.81 MPa, Southern Pump Co., Ltd., Shenzhen, China), and the pressure-regulating ball valve and the pressure-relief ball valve were used to set the reading of the pressure gauge (with a range of 0~0.6 MPa and an accuracy of 0.002 grade) to H (H = 0.04, 0.06, 0.08, 0.10, 0.12, and 0.15 MPa). When the pressure gauge readings stabilized, the valve was opened, and when the water discharge from the emitter stabilized, the water discharge from the emitter was collected with a catchment container. The catchment time was 5 min, the volume was measured with a measuring cylinder (accuracy of 1 mL), the catchment was repeated three times at the same H, and the average was taken to calculate the flow rate q of the water discharge from the emitter.



1. Mixer 2. Tank 3. Pump 4. Filter 5. Regulator ball valve 6. Pressure-relief ball valve 7. Pressure gauge 8. Valves 9. Emitter specimen 10. Receiving container

Figure 4. Schematic diagram of the test platform of the emitter.

2.4. Numerical Simulation

To carry out the rapid optimization design of the flow channel structure of the variable flow emitter, this study used Fluent 17.0. software to study hydraulic performance indices [29] such as q and the flow index (x) of the variable flow emitter, as well as the response law of the anticlogging performance indices, such as the internal flow velocity (v), turbulent kinetic energy (k), particle retention time (t), and particle passage rate (η) of the variable flow emitter to the structural parameters [53].

2.4.1. Grid Division

The integrated computer engineering and manufacturing code for computational fluid dynamics (ICEM CFD) was used to mesh the fluid region of the variable flow emitter [54], and an unstructured mesh was selected for the division method. Owing to the long and narrow structure of the three toothed channels and the zigzagging boundary, to simulate the flow of water and sand more accurately, the boundary layer mesh was set to 0.05 mm at channels a, c, and e, the remaining parts were set to 0.1 mm, and the number of meshes was 2.3~3.6 million.

2.4.2. Simulation Setup for Two-Phase Flow of Water and Sand

In this study, CFD was used to model both the fluid flow and the transport of sand particles through the emitter. The flow equations were solved using the Navier–Stokes equations for incompressible flow, while the sand particle dynamics were modeled using the discrete phase model (DPM). Its primary control equations [55] include the following:

The continuity equation:

$$\frac{\partial \rho}{\partial t} + \nabla \cdot (\rho u) = 0 \quad (1)$$

where ρ is the fluid density, and u is the fluid velocity vector.

The momentum equation:

$$\rho(\frac{\partial u}{\partial t} + u \cdot \nabla u) = -\nabla p + \mu \nabla^2 u + f \quad (2)$$

where ρ is the fluid density, u is the fluid velocity vector, p is the pressure, μ is the dynamic viscosity of the fluid, and f is the volumetric force

The particle motion equation:

$$mp\frac{dvp}{dt} = Fd + Fg + Fp \quad (3)$$

where m_p is the particle mass, v_p is the particle velocity, F_d is the drag force exerted by the fluid on the particle, F_g is the force of gravity, and F_p is the other acting force.

The turbulence model for the continuous-phase steady-state calculations was realizable k–ε [17], with the flow channel inlet pressures H set to 0.04, 0.06, 0.08, 0.10, 0.12, and 0.15 MPa, and the outlet pressure H' set to 0 MPa. The water–sand two-phase flow simulation was carried out after the continuous-phase steady-state calculation, and the discrete phase model (DPM) of the Euler–Lagrange method was selected. An interphase coupling algorithm was used to simulate the effect of the discrete phase (sand) on the continuous phase without considering other additional forces, such as the gradient force, spurious mass force, Saffman uplift force, thermophoretic swimming force, and Basset force. The boundary conditions of the inlet and outlet were set as "escape", and the wall boundary was set as "reflect". H was set as 0.10 MPa, H' was set as 0 MPa, the discrete phase particles were sand and silt, the density of the material was set as 2500 kg/m^3, and the diameter of the sand and silt particles was set as 0.05 mm. These particles were injected vertically at the surface of the inlet, and the sand particles were injected into the inlet at the same speed as the flow rate of the inlet water. Considering the particle diffusion caused by the turbulent pulsation of the fluid, a random orbit model was used to track the trajectory of the particles in the flow field under the Lagrangian coordinate system.

2.5. Testing, Simulation, and Calculation of Indicators

2.5.1. Emitter Flow and Flow Indices

The hydraulic performance tests under clear water conditions and Fluent simulation can be used to obtain the q for emitters with different combinations of flow channel structural parameters at H = 0.04~0.15 MPa, and the corresponding x can be obtained based on the exponential function relationship between q and H (Equation (4)).

$$q = kH^x \quad (4)$$

2.5.2. Simulation of the Flow Field and Sediment Particle Movement Inside the Emitter Flow Channel

CFD–post was used to monitor the change patterns of fluid flow velocity (v) and turbulent kinetic energy (k) between the trajectory of sediment particles and the position of 1/2 depth of the flow channel. Among them, k is an index that describes the energy in turbulent fluid motion, mainly from the time-averaged flow [53], which is driven by Reynolds shear; the larger k is, the more energy is extracted from the time-averaged flow, which is more conducive to promoting the transportation of sand particles in the flow channel, reducing the chances of retaining sand particles inside the flow channel and improving the anticlogging performance of the emitter [43,56]. The particle movement trajectory is the path of particles moving in the fluid. Through the particle retention time (t), the particle residence distribution in the flow channel and residence time can be determined and then analyzed to obtain the deposition of particles in the flow channel. η is the percentage of the number of particles n flowing out from the outlet of the flow channel to the number of particles N entering the flow channel, which can directly reflect the anticlogging performance of the emitter [45,57,58].

2.6. Model Validation

The agreement between the simulated and measured values of q corresponding to different H values under clear water conditions was evaluated via the normalized root mean square error (nRMSE), which was calculated as follows:

$$nRMSE = \sqrt{\frac{\sum_{i=1}^{n} (q_m - q)^2}{n \times {q_{ave}}^2}} \times 100\% \quad (5)$$

The *relative error* is the relative amount of error between the simulated value and the measured value, which is usually used to indicate the accuracy of the simulation results, and its calculation equation is as follows:

$$Relative\ Error = \frac{q_m - q}{q_m} \times 100\% \quad (6)$$

In Equations (5) and (6), q_m and q are the measured and simulated values when the system inlet pressure is H_i, respectively; q_{ave} is the average of the measured values; and n is the number of measured values. When nRMSE $\leq$ 10%, the simulation accuracy is very high; when 10% < nRMSE < 20%, the simulation accuracy is high; when 20% $\leq$ nRMSE $\leq$ 30%, the simulation accuracy is fair; and when nRMSE > 30%, the simulation accuracy is poor [59,60].

2.7. Data Analysis

The degree of influence on the indicators by the change in the level of the test factor can be obtained via extreme difference analysis to determine the optimal level of the factor and obtain the primary and secondary order of the influence indicators [61]. Based on the mathematical regression models of the hydraulic performance indices ($q_{0.1}$, x) and anticlogging performance indices (η) with channel structural parameters (E, B, A, D), the optimized combination of channel structural parameters to meet different demands can be quickly determined via the scipy.optimize.minimize function.

In the model, $p < 0.05$ means that the effect of the regression coefficients of the test factors on the regression equation of the indicator reached the level of significance, and $p > 0.05$ means that the effect of the test factors on the regression equation of the indicator did not reach the level of significance. All the data were analyzed via IBM SPSS Statistics 26 (International Business Machines Corporation, USA) and plotted via Microsoft Office Excel 2016 (Microsoft Corporation, Washington, DC, USA) software.

3. Results

3.1. Model Validation

The q_m and q values of 10# emitter at H = 0.04~0.15 MPa under clear water conditions are shown in Table 2. The nRMSE of the measured and simulated values is 11.23%, the *relative error* is 5.65~14.98%, the *relative error* of the measured value of the flow index x_m and the simulated value of x is 4.8%, and the clear water conditions have a high Fluent simulation accuracy.

Table 2. Measured (q_m) and simulated (q) flow rates and flow index (x) of 10# emitter under different pressures (H).

Norm	*H*/MPa						*x*
	0.04	**0.06**	**0.08**	**0.10**	**0.12**	**0.15**	
$q_m/(L \cdot h^{-1})$	1.02	1.24	1.47	1.64	1.84	2.07	
$q/(L \cdot h^{-1})$	0.96	1.17	1.34	1.50	1.64	1.76	
Relative Error/%	5.88	5.65	8.84	8.54	10.87	14.98	
nRMSE/%			11.23				
x_m			/				0.515
x			/				0.491
Relative Error/%			/				4.66

3.2. Hydraulic Performance of Emitters

The $q_{0.1}$ values of the variable flow emitter volumes from 1# to 9# ranged from 1.05 to 2.22 L/h, and x ranged from 0.487 to 0.515, with x being the smallest for the 4# and 8# emitters and the largest for the 6# emitter (Table 3).

Table 3. Simulation results of emitter flow rate (q) and flow index (x) under different pressures (H).

Trial Number	$q/(L \cdot h^{-1})$						*x*
	***H* = 0.04 MPa**	***H* = 0.06 MPa**	***H* = 0.08 MPa**	***H* = 0.10 MPa**	***H* = 0.12 MPa**	***H* = 0.15 MPa**	
1	0.67	0.82	0.94	1.05	1.15	1.29	0.498
2	1.03	1.27	1.46	1.63	1.79	2.00	0.500
3	1.39	1.71	1.98	2.22	2.43	2.72	0.508
4	1.16	1.41	1.63	1.81	1.98	2.21	0.487
5	0.71	0.87	1.00	1.12	1.22	1.36	0.493
6	1.05	1.30	1.50	1.69	1.85	2.08	0.515
7	0.89	1.08	1.25	1.39	1.52	1.69	0.489
8	1.19	1.45	1.67	1.86	2.04	2.27	0.487
9	0.75	0.92	1.06	1.18	1.29	1.45	0.492

The extreme difference analysis of the hydraulic performance of the emitter is shown in Table 4. A larger range value indicates that a change in this test factor within the design range will lead to a greater change in the numerical value of the test index and a greater degree of influence of this factor on the hydraulic performance of the emitter. The order of influence of each factor on $q_{0.1}$ is D > B > E > A, and the order of influence on x is B > E > D > A. Factor A is at the end of the order of influence of the two indicators, and its influence on the hydraulic performance of the emitter is the smallest.

Table 4. Polar analysis of the flow rate ($q_{0.1}$) versus x for the emitter at 0.1 MPa.

Test Indicators		Structural Parameters			
		E/mm	**B/mm**	**A/°**	**D/mm**
$q_{0.1}$	$q_{0.1\,1}$	1.63	1.42	1.53	1.12
	$q_{0.1\,2}$	1.54	1.54	1.57	1.57
	$q_{0.1\,3}$	1.48	1.70	1.54	1.96
	R_q	0.16	0.28	0.04	0.85
x	x_1	0.5022	0.4912	0.4999	0.4943
	x_2	0.4983	0.4934	0.4967	0.5012
	x_3	0.4892	0.5050	0.4930	0.4941
	R_x	0.0130	0.0138	0.0070	0.0071

Note: R_q and R_x denote the polar deviations of different structural parameters under different determination indices.

Taking the test factors as the horizontal coordinates and the test indices as the vertical coordinates (Figure 5), $q_{0.1}$ was negatively correlated with E, positively correlated with B and D, and changed less with A. x was positively correlated with B, negatively correlated with E and A, and tended to increase and then decrease with D.

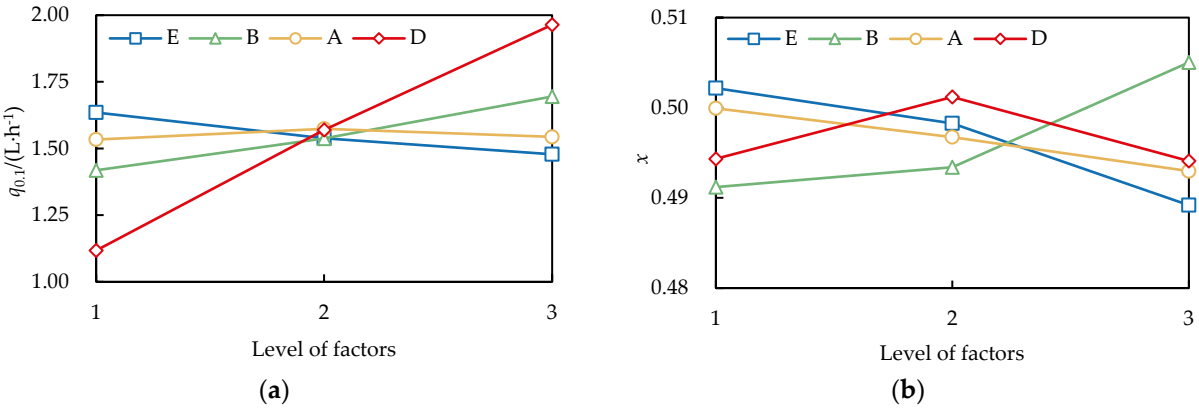


Figure 5. Effects of different factor levels on $q_{0.1}$ (**a**) and x (**b**).

3.3. Flow Field and Particle Motion Characteristics Inside the Emitter Flow Channel

The flow velocity vector distributions of the 4# emitters ($q_{0.1}$ = 1.81, x = 0.487) and 8# emitters ($q_{0.1}$ = 1.86, x = 0.487), which had the smallest x, as well as the 3# emitters ($q_{0.1}$ = 2.22, x = 0.508) and the 6# emitters ($q_{0.1}$ = 1.69, x = 0.515), which had x > 0.50, were selected for the deeper 1/2 position of channel a. Starting from the third channel cell at the inlet of channel a, five channel cells were taken for local analysis (Figure 6). The distribution law of the flow velocity vector in each channel unit was similar: the main flow area was concentrated mainly near the tooth tip on the water surface, which presented peak and trough flow states under the influence of the channel structure. At the same time, owing to the role of its own inertia, the peak and trough of the fluid and the toothed structure of the channel tended to follow each other. The maximum flow velocities v_{max} of these four groups of emitters were 3.49, 3.35, 3.85, and 3.73 m/s, respectively; the average flow velocity v was 0.701, 0.656, 0.799, and 0.704 m/s, respectively; and the order was 3# > 6# > 4# > 8#.

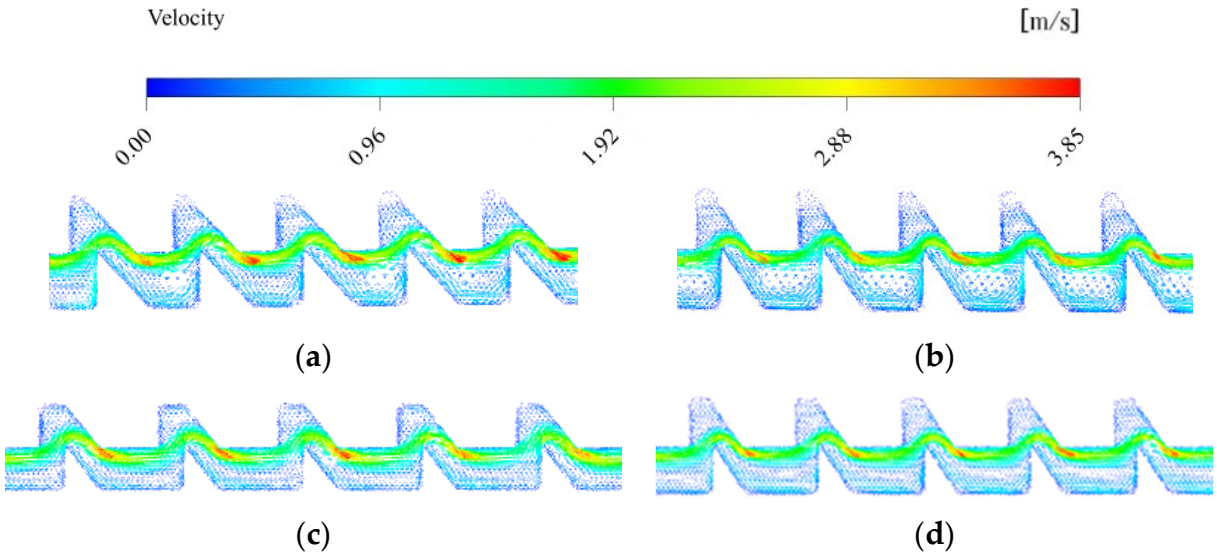


Figure 6. Velocity vector distributions at the 1/2 depth position of the channel for emitters 4# (**a**), 8# (**b**), 3# (**c**), and 6# (**d**).

The turbulent kinetic energy distribution of the four groups of emitters at the deep 1/2 position of the channel structure is shown in Figure 7. The low turbulent kinetic energy (<0.1 m^2/s^2) flow area was mainly at the bottom of the channels at the baffle wall surface and tooth corners. The 3# emitter had the smallest area of low turbulent kinetic energy flow area in channel a. The area of the turbulent kinetic energy of the various emitters that was less than 0.1 m^2/s^2 was 44.05%, 52.57%, 22.42%, and 40.55%, and the order was 8 # > 4 # > 6 # > 3 #. High turbulent kinetic energy accounted for a larger proportion of 6 #, and the 3 # channel tooth spacing was the same as that of the other 2.2 mm emitters. The average turbulent kinetic energy k values for 4 #, 8 #, 3 #, and 6 # in channel a were 0.170, 0.142, 0.227, and 0.172 m^2/s^2, and the order was 3 # > 6 # > 4 # > 8 #.

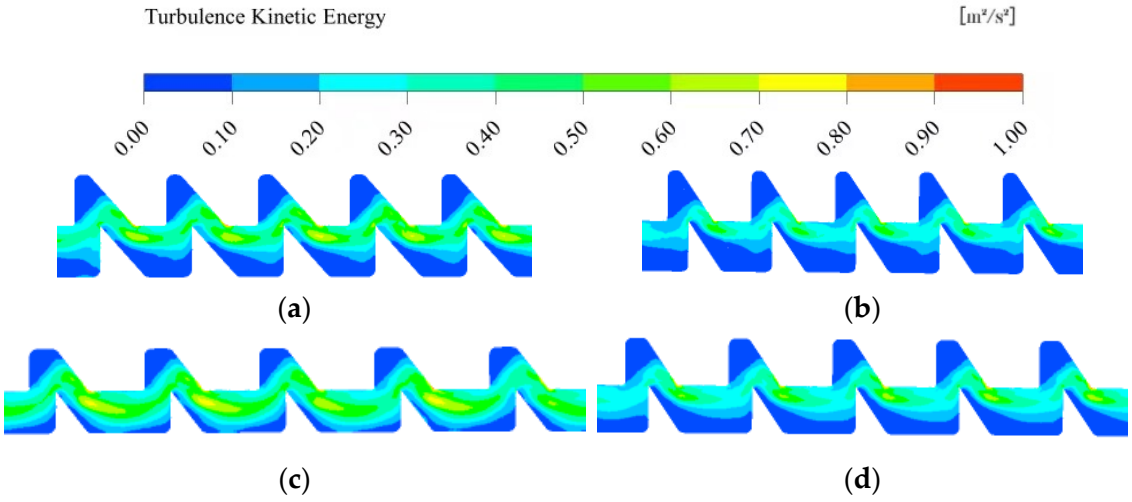


Figure 7. Turbulent kinetic energy distributions at the 1/2 depth position of the channel for emitters 4# (**a**), 8# (**b**), 3# (**c**), and 6# (**d**).

The particle motion trajectory of a single particle in the localized flow channel of four groups of emitters with different variable specifications is shown in Figure 8. The retention time of the particles in the flow channel increases with increasing particle motion distance in the flow channel. The particles appeared to turnover more when entering the 4# and 8# emitters, the particle motion turnover in the 4# emitter was near the bottom water-retaining wall surface, and the particle motion turnover in the 8# emitter appeared at the tip of the tooth. The maximum retention times t corresponding to the particle motion trajectories in channels 4#, 8#, 3#, and 6# were 0.44, 0.52, 0.18, and 0.41 s, respectively, in the following order: 3# < 6# < 4# < 8#.

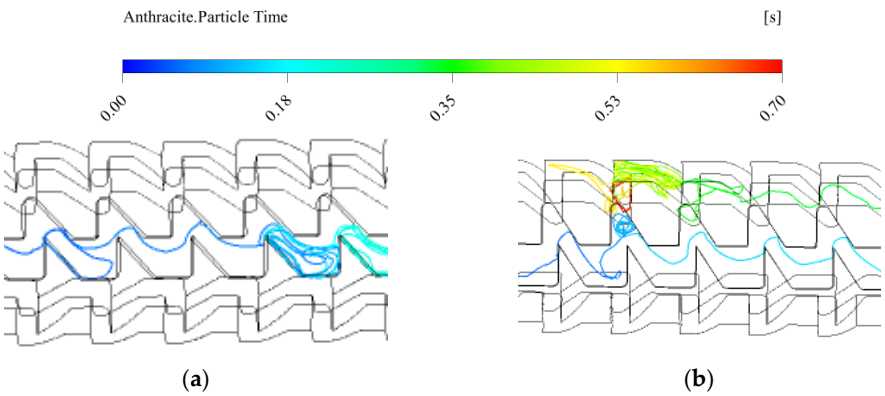
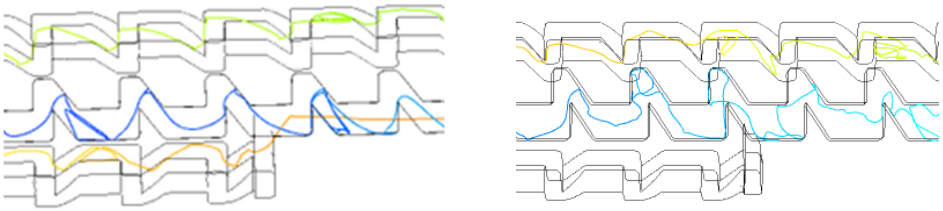


Figure 8. *Cont.*



(**c**) (**d**)

Figure 8. Plots of individual particle trajectories versus retention times for the 4# (**a**), 8# (**b**), 3# (**c**) and 6# emitter (**d**) flow paths.

3.4. Analysis of the Relationship Between the Anticlogging Performance and Hydraulic Performance of Water Emitters

The order of the effect of each factor on η was E > B > D > A (Table 5). In the water–sand two-phase flow simulation, the η values of different sizes of variable flow emitters ranged from 77.38% to 99.88%, among which the 3# emitter was the largest and the 8# emitter was the smallest, and the η rankings of the 4#, 8#, 3#, and 6# flow channels were the same as those for the average turbulent kinetic energy of the flow channels, and the time of the particles retained in the flow channels became shorter with increasing particle passage rates. The η of the variable flow emitter is quadratically related to $q_{0.1}$ (R^2 = 0.1284) (Figure 9a), and η is quadratically related to x, with a coefficient of determination R^2 of 0.8883 (Figure 9b). In operating stage I, the anticlogging performance of the variable flow emitter increased and then decreased with hydraulic performance, and η reached its maximum value when x = 0.5055. The η of the variable flow emitter had a linear relationship with both v and k, and the coefficients of determination R^2 were 0.5587 and 0.4632, respectively (Figure 9c,d).

Table 5. Polar analysis of the particle passage rate (η) in the emitters.

Test Indicators		Structural Parameters			
		E/mm	B/mm	A/°	D/mm
η_i (%)	η_1 (%)	96.14	85.48	90.43	91.73
	η_2 (%)	90.29	88.49	88.31	93.14
	η_3 (%)	83.33	95.78	91.02	84.89
	R_η (%)	12.81	10.30	2.71	8.25

Note: η_i denotes the mean value of the particle passage rate at different levels of structural parameters; R_η denotes the extreme deviation of different structural parameters under the measurement index.

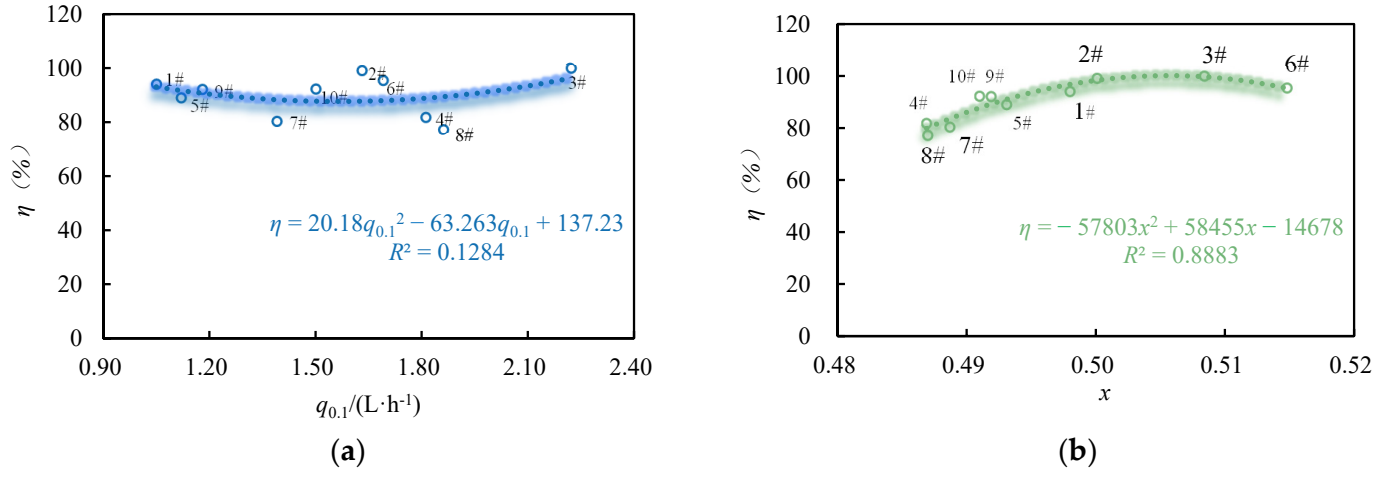


Figure 9. *Cont.*

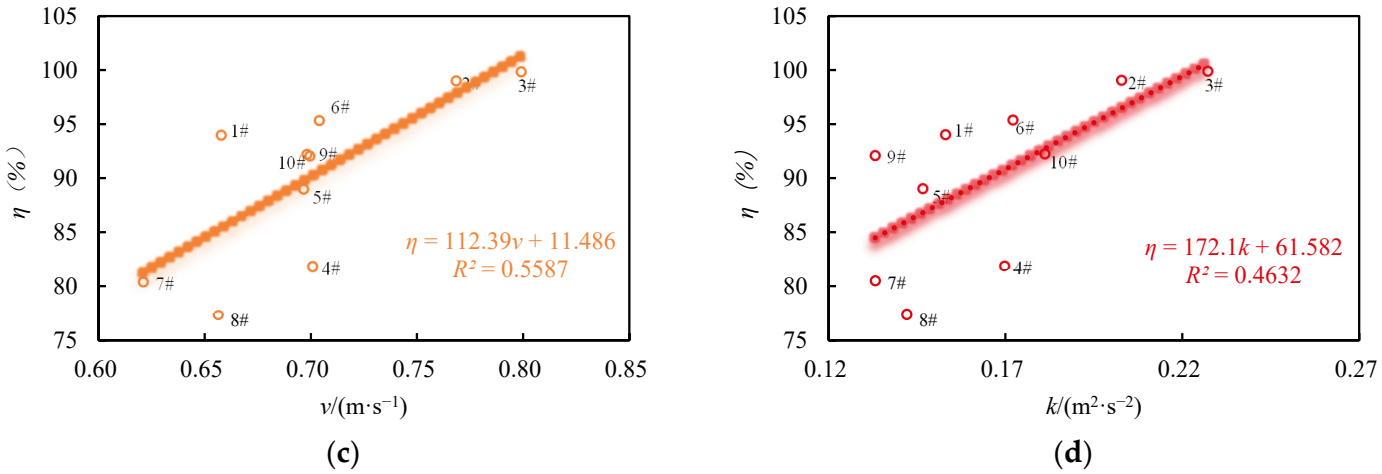


Figure 9. Variation in η of the emitter with simulation results of $q_{0.1}$ (**a**), x (**b**), v (**c**), and k (**d**).

3.5. Optimization of the Structural Parameters of Variable Flow Emitter Flow Paths

3.5.1. Modeling of Hydraulic Performance and Anticlogging Performance Indicators of Emitters in Relation to Structural Parameters

The data were analyzed by linear regression through SPSS 26.0. The regression model determination coefficients R^2 of $q_{0.1}$ and η with each structural parameter were 0.995 and 0.875, respectively, with high fitting accuracy, whereas the regression model determination coefficient R^2 of x with each structural parameter was 0.79, with low fitting accuracy. The effects of the constant term and the regression coefficients of E, B, and D on the multiple linear regression equations of $q_{0.1}$ and η reached the significance level ($p < 0.05$), whereas the effect of A on the linear regression equations of $q_{0.1}$ and η did not reach the significance level ($p > 0.1$). The effects of the constant term, as well as the linear regression equations of E and B on x, reached the significance level ($p < 0.05$), whereas the effects of both A and D on the linear regression equation of x did not reach the level of significance ($p > 0.1$). The constant term did not reach the level of significance for the linearity of the flow channel ($p > 0.1$), and the remaining structural parameters had a significant effect on the linear regression equation of this indicator ($p < 0.05$) (Table 6). To simplify the nonlinear regression model expression, Factor A was excluded from the regression model for the flow index. Regression models of $q_{0.1}$, x, and η with the flow channel structural parameters E, B, A, and D were developed for 10 specification variables irrigators, respectively (Table 7).

Table 6. Significance analysis of regression coefficients of regression models for the rated flow rate, flow index, and particle passage rate of emitter channels.

Norm	Regression Coefficient	Unstandardized Coefficient B	Unstandardized Coefficient Standard Error	Standardized Coefficient Beta	*t*-Value	*p*-Value	VIF
$q_{0.1}$	Constant term	−1.175	0.205		−5.720	0.002	
	E/mm	−0.394	0.064	−0.186	−6.118	0.002	1.031
	B/mm	0.689	0.064	0.326	10.689	0.000	1.031
	A/°	0.001	0.003	0.013	0.413	0.697	1.031
	D/mm	2.115	0.068	0.933	31.088	0.000	1.000
	R^2			0.995			
	F			276.232			
	p			**			

Table 6. *Cont.*

Norm	Regression Coefficient	Unstandardized Coefficient B	Unstandardized Coefficient Standard Error	Standardized Coefficient Beta	*t*-Value	*p*-Value	VIF
x	Constant term	0.493	0.035		13.908	0.000	
	E/mm	−0.031	0.011	−0.578	−2.778	0.039	1.031
	B/mm	0.035	0.011	0.655	3.148	0.025	1.031
	A/°	−0.001	0.001	−0.343	−1.648	0.160	1.031
	D/mm	−0.001	0.012	−0.015	−0.071	0.946	1.000
	R^2			0.79			
	F			4.696			
	p			*			
η	Constant term	0.745	0.148		5.049	0.004	
	E/mm	−0.354	0.046	−0.794	−7.657	0.001	1.031
	B/mm	0.261	0.046	0.586	5.647	0.002	1.031
	A/°	0.002	0.002	0.109	1.052	0.341	1.031
	D/mm	−0.133	0.049	−0.279	−2.73	0.041	1.000
	R^2			0.948			
	F			22.716			
	p			**			

Note: * and ** represent $p < 0.1$ and $p < 0.05$, respectively.

Table 7. Mathematical regression model of variable flow emitters $q_{0.1}$, x, and η with flow channel structural parameters.

$q_{0.1} = -1.175 - 0.394\ E + 0.689\ B + 0.001\ A + 2.115\ D$	$R^2 = 0.995$	(7)
$x = 0.411 - 0.005\ E^2 + 0.051\ B^2 - 0.115\ D^2 - 0.087\ EB + 0.332\ ED - 0.007\ BD - 0.075\ EBD$	$R^2 = 0.883$	(8)
$\eta = 0.745 - 0.354\ E + 0.261\ B + 0.002\ A - 0.133\ D$	$R^2 = 0.948$	(9)

3.5.2. Preferred Combination of Structural Parameters for Emitter Channels

Based on Equations (7)–(9), the combination of $q_{0.1}$, hydraulic performance, and the anticlogging performance of the variable flow emitter channel structure parameters required for drip irrigation systems can be quickly obtained using the minimize function in SciPy library and Python software 3.8.0. This can be performed according to the water conditions, engineering inputs, crop water consumption, and soil conditions of the actual project. Taking $q_{0.1}$ = 1.5, 2.0 L/h as an example, the constraints are as follows: 0.6 mm $\leq$ E $\leq$ 1.0 mm, ΔE = 0.1 mm; 1.8 mm $\leq$ B $\leq$ 2.2 mm, ΔB = 0.1 mm; 34° $\leq$ A $\leq$ 42°, ΔA = 1°; and 0.6 mm $\leq$ D $\leq$ 1.0 mm, ΔD = 0.1 mm. The objective function represents the goal of the optimization, typically a performance metric you want to minimize or maximize. The optimization objectives are Min x, Max η, and Min M. For Min M, M = 0.5 x–0.5 η when the weights of both hydraulic performance and clogging resistance are 0.5 (Equation (10)). x minimum, η maximum, and the combinations of flow channel structural parameters under the three optimization objectives of considering x and η at the same time are shown in Table 8.

The structural parameter combinations of Min x usually pertained to the reduction of cost or loss, and the x obtained for the rated flow rates of 1.5 and 2.0 L/h were lower at 0.500 and 0.484, respectively. The structural parameter combinations of Max η were usually concerned with the improvement of efficiency, and the rated flow rates of 1.5 and 2.0 L/h obtained by η were higher at 98.80% and 96.62%, respectively. The structural parameter combination of Min M was the result of the balance of the comprehensive consideration of x and η, and the rated flow rates of 1.5 and 2.0 L/h obtained by x were 0.501 and 0.484, respectively, and those obtained by η were 92.86% and 95.34%, respectively.

Table 8. Preferred combinations of channel structure parameters.

Optimization Solutions	Emitter Specifications	Channel Structure Parameters				x	η/%
	$q_{0.1}$/(L·h^{-1})	E/ mm	B/ mm	A/°	D/mm		
Min x	1.5	0.8	1.8	42	0.8	0.500	90.92
	2.0	0.6	1.8	42	1.0	0.484	95.34
Max η	1.5	0.6	2.0	42	0.7	0.529	98.80
	2.0	0.7	2.2	36	0.9	0.533	96.62
Min M	1.5	0.7	1.8	34	0.8	0.501	92.86
	2.0	0.6	1.8	42	1.0	0.484	95.34

$$M = 0.166\,ED - 0.0435\,EB - 0.0035\,BD - 0.0375\,EBD - 0.0025\,E^2 + 0.0255\,B^2 - 0.0575\,D^2 + 0.177\,E - 0.1305\,B - 0.001\,A + 0.0665\,D - 0.167 \quad (10)$$

4. Discussion

This study explores the response of hydraulic performance and anticlogging performance to changes in key structural parameters, leveraging numerical simulation techniques and advanced turbulence models to analyze flow behavior. The findings offer insights into emitter performance under various practical conditions, providing valuable guidelines for the design and application of variable flow emitters in different agricultural environments.

4.1. Law of Response of the Hydraulic Performance of a Variable Flow Emitter to Structural Parameters

Based on the realizable k–ε turbulence model in Fluent software, the *nRMSE* between the measured and simulated values of q for the variable flow emitter at operating stage I (Figure 1a) is less than 15%, with a high simulation accuracy, and the *relative error* between the measured and simulated values of q and x is 4.66–14.98%, which is similar to the range of accuracy in existing studies [62–64]. In the studies by Xing et al. [64] and Xu and Zhang [65], the measured value of q was lower than the simulated value because of the insufficient smoothness of the sidewalls of the emitter sample, which was made of Plexiglas material and used CNC machine tool machining technology, and the low machining accuracy of the emitter flow channel, which resulted in additional energy dissipation when the water flow moved in the flow channel. In this study, the effects of mass force and channel wall roughness were considered in the simulation of the emitter. At the same time, the variable flow emitter core was processed from stainless steel, which has a smooth surface and is more scratch-resistant than Plexiglas. The elastomer of the variable flow emitter was selected from Teflon rigid tubes, which led to slight deformation of the elastomer during the water flow movement inside the channel, such that the measured value of q was higher than the simulated value.

In this study, a numerical simulation study was carried out for the tooth height (E), tooth spacing (B), tooth angle (A), and channel depth (D) of the channels. The order of structural parameters affecting $q_{0.1}$, x was obtained by polar analysis as follows: D > B > E > A, B > E > D > A, and A was found to have the smallest effect on $q_{0.1}$, x. In the existing studies on emitter channels, no consistent conclusions on the order of influence of the channel structural parameters on $q_{0.1}$, x were obtained, and the primary and secondary order of the influence of each parameter on the performance indices varied owing to differences in emitter types, the range of structural parameter selection, etc. [29,30,32,66]. Therefore, for different types of emitters, it is necessary to explore the effects of flow channel structural parameters on their hydraulic performance.

4.2. Changes in the Internal Flow Field and Anticlogging Performance of the Water Emitter

The area of the region in the flow channel with turbulent kinetic energy less than 0.1 m^2/s^2 as well as t tended to decrease with increasing v and k. η was positively correlated with v and k. Similarly, Yang et al. [43] and Xu et al. [65] reported that adjusting the tooth

shape to reduce the area of the low-flow velocity zone, increasing the k of the main flow zone, and increasing the ability of particles to gain access to the outside can increase the rate of particle transport, reduce t, and decrease sedimentation and deposition; these studies also reported that emitter flow paths are susceptible to clogging in the low-flow velocity zone [67]. Fully considering the distribution characteristics of vortices in the flow channel, abating the low-flow zone can improve its anticlogging performance [68,69], whereas increasing the v of the emitter can improve its anticlogging performance [70].

A study by Gao et al. [17] focused only on the optimization of the hydraulic performance of variable flow emitters at the stage of regular-flow water supply, without considering the improvement in anticlogging performance. Currently, η was selected as the evaluation index for the anticlogging performance of the emitter, and in our study, the range of η was from 77.38% to 99.88%, which was basically within the range of η values (50% to 99%) in existing studies [38,71]. Some scholars have shown that the different emitter flow channel parameters, operating pressures, and sand particle sizes have an influence on η [72,73]. In our study, the order of influence of the emitter channel structure parameters on η was E > B > D > A. In addition, for different channel structure forms, different key parameters were selected. The order of the parameters affecting η was also different, e.g., turning angle of tooth > channel width/channel depth > width of tooth top / channel tooth height > channel tooth height/channel width [58] and vortex circle radius > arc circle center to vortex circle center connecting line > vortex circle spacing > internal arc radius [74].

In this study, η tends to increase and then decrease with increasing x (Figure 9b) and reaches its maximum value when x = 0.5055. Studies have shown that x increases with decreasing water flow turbulence degrees in the flow channel [75,76]. The greater the degree of turbulence in a certain range of water flow is, the greater the wall surface shear force in the flow channel and the stronger the turbulence kinetic energy, which is conducive to promoting the transportation of sand particles in the flow channel, reducing the retention of sand particles inside the flow channel, and improving the anticlogging performance of the emitter [43,53,56]. In general, there is a contradiction between the hydraulic performance and the clogging resistance of variable flow emitters.

To this end, multiple linear regression equations of $q_{0.1}$, x, η, and flow channel structural parameters were constructed, and the optimal combinations of Min x, Max η, and Min (0.5 x–0.5 η) flow channel structure parameters for each of the three scenarios were obtained: (1) cases of cleaner water sources, food crops (such as wheat and corn), and the need to reduce the unit area investment for drip irrigation systems in large-scale projects requiring the long-distance laying of driplines; (2) scenarios with water sources containing significant sediment or suspended matter, or where stable operation with minimal maintenance over a long period is required, are suitable for cash crops, such as apples, cherries, and grapes; and (3) integrated irrigation systems that require simultaneous attention to both hydraulic uniformity and system stability. Dripline design and manufacturing can be based on the actual agricultural environment (e.g., water conditions and soil texture) and irrigation needs, as well as the weights of the flow rate, flow index, and particle passage rate of each emitter design, and these weights can be changed to meet the different requirements of each combination of emitter structure parameters. The goal is to increase the application area of subsurface drip irrigation and enhance the potential for water conservation in agriculture.

Optimizing parameters for testing in different soil types is critical for subsurface irrigation systems, as soil characteristics, such as texture and permeability, can significantly affect their performance. In future studies, we will test these parameters across various soil types to enhance the applicability of our findings.

5. Conclusions

This paper focuses on a variable flow emitter as the research object, utilizing experimental tests, CFD numerical simulations, and flow channel structure optimization to explore the intrinsic connections between the comprehensive performance and structural parameters of a variable flow emitter. The study aims to provide a scientific basis for further

research on variable flow emitter products and promote their engineering applications. The main conclusions are as follows:

1. The realizable *k–ε* turbulence model and the discrete phase model can be used to carry out studies of numerical simulations within the emitter flow channel;
2. The *nRMSE* between the measured and simulated values of the water outlet flow from the emitter is 11.23%, and the Fluent simulation accuracy is high;
3. The results of the polar variance analysis reveal that the influence of the flow channel structural parameters on the flow index is in the order of B > E > D > A, the influence on the flow rate is in the order of D > B > E > A, and the influence on the particle passage rate is in the order of E > B > D > A;
4. The proportion of the low turbulent kinetic energy flow area is negatively correlated with the flow velocity, the retention time of the particles in the flow channel is positively correlated with the proportion of the low turbulent kinetic energy flow area, and the passage rate of the particles is positively correlated with the mean flow velocity and mean turbulent kinetic energy;
5. Based on the multivariate linear regression model of hydraulic performance and anti-clogging performance evaluation indices and structural parameters, the combinations of variable flow emitter channel structural parameters required for drip irrigation systems under different working conditions were obtained via the minimization function.

Author Contributions: Conceptualization, Y.M.; methodology, P.N. and Y.M.; software, P.N.; val–idation, Y.M. and B.Y.; formal analysis, P.N., Z.Y., Y.Z. and D.Z.; investigation, P.N. and Y.M.; writing—original draft preparation, P.N.; writing—review and editing, Y.M. and B.Y.; funding acqui–sition, Y.M. and B.Y. All authors have read and agreed to the published version of the manuscript.

Funding: This research was funded by the Key Science and Technology Project for Revitalization of Inner Mongolia, China (2022EEDSKJXM004), the Research and Development Support Program of China Institute of Water Resources and Hydropower Research (ID0145B042021), the Inner Mongolia Autonomous Region Key Research and Transformation of Achievements Program (2022YFHH0030), the earmarked fund for XJARS-Cotton (XJARS-03), and the Graduate Student Research Innovation Program of Tarim University (TDGRI202252).

Data Availability Statement: The data presented in this study are available upon request from the corresponding author.

Acknowledgments: We thank the College of Water Conservancy and Architectural Engineering of Tarim University, the State Key Laboratory of Simulation and Regulation of Water Cycle in River Basin, and the China Institute of Water Resources and Hydropower Research for their support and cooperation in this project.

Conflicts of Interest: The authors declare no conflicts of interest.

Abbreviations

The following abbreviations are used in this manuscript:

CFD	Computational fluid dynamics
Realizable *k–ε*	Realizable k-epsilon turbulence model
nRMSE	Normalized root mean square error
q_m	Measured flow rate, (L·h^{-1})
q	Simulated flow rate, (L·h^{-1})
x_m	Measured flow index
x	Simulated flow index
$q_{0.1}$	Simulated flow rate at 0.1 MPa, (L·h^{-1})
η	Particle passage rate, (%)
t	Particle retention time, (s)
A	Tooth angle

E	Tooth height
B	Tooth spacing
D	Flow channel depth
v	Flow velocity, ($m \cdot s^{-1}$)
k	Turbulent kinetic energy, ($m^2 \cdot s^{-2}$)
SDI	Subsurface drip irrigation
PIV	Particle image velocimetry
CNC	Computer numerical control
DPM	Discrete phase model
H	Inlet pressures, (MPa)
R^2	Coefficient of determination

References

1. Hua, H.; Kang, S. The economic and environmental effect of subsurface drip irrigation. *Acta Univ. Agric. Boreali-Occident.* **2000**, *28*, 79–83.
2. Lamm, F.R.; Trooien, T.P. Subsurface drip irrigation for corn production: A review of 10 years of research in Kansas. *Irrig. Sci.* **2003**, *22*, 195–200. [CrossRef]
3. Lamm, F.R.; O'Brien, D.M.; Rogers, D.H. Economic comparison of subsurface drip and center pivot sprinkler irrigation using spreadsheet software. *Appl. Eng. Agric.* **2015**, *31*, 929–936. [CrossRef]
4. Li, J.; Yang, F.; Li, Y. Water and nitrogen distribution under subsurface drip fertigation as affected by layered–textural soils. Trans. Chin. *Soc. Agric. Eng.* **2009**, *25*, 25–31.
5. Mo, Y.; Li, G.; Wang, D.; Lamm, F.R.; Wang, J.; Zhang, Y.; Cai, M.; Gong, S. Planting and preemergence irrigation procedures to enhance germination of subsurface drip irrigated corn. *Agric. Water Manag.* **2020**, *242*, 106412. [CrossRef]
6. Cao, X.; Feng, Y.; Li, H.; Zheng, H.; Wang, J.; Tong, C. Effects of subsurface drip irrigation on water consumption and yields of alfalfa under different water and fertilizer conditions. *J. Sens.* **2021**, *1*, 6617437. [CrossRef]
7. Guo, S.; Mo, Y.; Wu, Z.; Wang, J.; Zhang, Y.; Gong, D.; Xu, M.; Guo, B.; Shen, X. The Effects of Furrow Depth in Alternate Row Planting on Germination and Yield of Spring Maize under Subsurface Drip Irrigation in North China Plain. *J. Irrig. Drain.* **2021**, *40*, 27–34. [CrossRef]
8. Mo, Y.; Zhang, Y.; Wang, D.; Wang, J.; Li, G.; Gong, S.; Gao, X. Germination and growth of corn submitted to sowing and cultivation management by subsurface drip irrigation in the North China Plain. *Irrig. Sci.* **2024**, *42*, 801–813. [CrossRef]
9. Muhammad, T.; Zhou, B.; Puig–Bargu, J.; Ding, C.; Li, S.; Manan, I.; Zhou, Y.; Liu, Z.; Li, Y. Assessment of emitter clogging with multiple fouling and root intrusion in sub–surface drip irrigation during 5–year sugarcane growth. *Agric. Water Manag.* **2022**, *274*, 107981. [CrossRef]
10. Camp, C.R.; Lamm, F.R. Irrigation systems, subsurface drip. *Encycl. Water Sci.* **2003**, 560–564.
11. Kandelous, M.M.; Šimůnek, J. Numerical simulations of water movement in a subsurface drip irrigation system under field and laboratory conditions using HYDRUS–2D. *Agric. Water Manag.* **2010**, *97*, 1070–1076. [CrossRef]
12. Schiavon, M.; Serena, M.; Leinauer, B.; Sallenave, R.; Baird, J.H. Seeding date and irrigation system effects on establishment of warm–season turfgrasses. *Agron. J.* **2015**, *107*, 880–886. [CrossRef]
13. Mo, Y.; Li, G.; Wang, D. A sowing method for subsurface drip irrigation that increases the emergence rate, yield, and water use efficiency in spring corn. *Agric. Water Manag.* **2017**, *179*, 288–295. [CrossRef]
14. Mo, Y.; Li, G.; Cai, M.; Wang, D.; Xu, X.; Bian, X. Selection of suitable technical parameters for alternate row/bed planting with high maize emergence under subsurface drip irrigation based on HYDRUS–2D model. *Trans. Chin. Soc. Agric. Eng.* **2017**, *33*, 105–112. [CrossRef]
15. O'Brien, D.M.; Rogers, D.H.; Lamm, F.R.; Clark, G.A. An economic comparison of subsurface drip and center pivot sprinkler irrigation systems. *Appl. Eng. Agric.* **1998**, *14*, 391–398. [CrossRef]
16. Mo, Y.; Wang, J.; Zhang, Y.; Li, Q.; Gong, S.; Xu, D.; Gao, X. Drip Irrigation Apparatus and System. US Patent US202117525055, 12 May 2022.
17. Gao, N.; Mo, Y.; Wang, J.; Yang, L.; Gong, S. Effects of Flow Path Geometrical Parameters on the Hydraulic Performance of Variable Flow Emitters at the Conventional Water Supply Stage. *Agriculture* **2022**, *12*, 1531. [CrossRef]
18. Li, G.; Wang, J.; Alam, M.; Zhao, Y. Influence of geometrical parameters of labyrinth flow path of drip emitters on hydraulic and anti–clogging performance. *Trans. ASABE* **2006**, *49*, 637–643. [CrossRef]
19. Li, Y.; Yang, P.; Xu, T.; Ren, S.; Lin, X.; Wei, R.; Xu, H. CFD and digital particle tracking to assess flow characteristics in the labyrinth flow path of a drip irrigation emitter. *Irrig. Sci.* **2008**, *26*, 427–438. [CrossRef]
20. Camp, C.R. Subsurface drip irrigation: A review. *Trans. ASABE* **1998**, *41*, 1353–1367. [CrossRef]
21. Yıldırım, G.; Ağıralioğlu, N. Linear solution for hydraulic analysis of tapered microirrigation laterals. *J. Irrig. Drain. Eng.* **2004**, *130*, 78–87. [CrossRef]
22. Li, Y.; Yang, P.; Xu, T.; Liu, H.; Liu, H.; Xu, F. Hydraulic property and flow characteristics of three labyrinth flow paths of drip irrigation emitters under micro-pressure. *Trans. ASABE* **2009**, *52*, 1129–1138. [CrossRef]

23. Pan, Y. Experimental Study on the Effect of Tooth Flow Structure on the Hydraulic Performance of Emitter Drip. Master's Thesis, Northwest A&F University, Xianyang Yangling, China, 2017.
24. Chang, Y.; Niu, W.; Wang, W. Numerical simulation and flow analysis of labyrinth path of drip irrigation emitters. *J. Northwest A&F Univ. (Nat. Sci. Ed.)* **2009**, *37*, 203–208. [CrossRef]
25. Xie, Q.; Niu, W.; Li, L. Effect of tooth angle and pitch of labyrinth channel on performance of emitter. *J. Drain. Irrig. Mach. Eng.* **2013**, *31*, 449–455. [CrossRef]
26. Chen, X.; Wu, P.; Fan, X.; Niu, W. Numerical simulation of structural parameters using CFD and anti–clogging design analyse on drip emitter. *J. Irrig. Drain.* **2008**, *27*, 35–38. [CrossRef]
27. Zhang, C.; Niu, Y.; Liu, X. Numerical simulation of influence of tooth angle on hyaraulic characteristics of labyrinth emitter. *J. Drain. Irrig.* **2022**, *40*, 751–756. [CrossRef]
28. Wang, J.; Gong, S.; Li, G.; Zhao, Y. The influence of geometrical parameters of dental flow passage of labyrinth emitter on the hydraulic performance under low working pressure. *J. Hydraul. Eng.* **2014**, *45*, 72–78. [CrossRef]
29. Zhang, L.; Li, S. Numerical experimental investigation of douche hydraulic performance on drop irrigation of tooth-type labyrinth channel. *Int. J. Hydroelectr. Energy* **2017**, *35*, 103–106.
30. Yang, B.; Zhang, G.; Wang, J.; Gong, S.; Wang, H.; Mo, Y. Numerical simulation of hydraulic performance of tooth–form channel of labyrinth emitter. *J. Irrig. Drain.* **2019**, *38*, 71–76. [CrossRef]
31. Liu, C.; Tang, D.; Zheng, J.; Zhou, H. Optimization of hydraulic performance for drip irrigation trapezoidal labyrinth channel of emitter using response surface methodology. *Trans. Chin. Soc. Agric. Eng.* **2011**, *27*, 46–51. [CrossRef]
32. Liu, C.; Tang, D.; Wang, L.; Zhao, Z. Multi output optimization of the hydraulic performance for drip irrigation trapezoidal labyrinth channel of emitter. *Arid. Land. Geogr.* **2016**, *39*, 600–606. [CrossRef]
33. Li, J.; Chen, L.; Li, Y. Field evaluation of emitter clogging in subsurface drip irrigation system. *J. Hydraul. Eng.* **2008**, *39*, 1272–1278. [CrossRef]
34. Wang, H.; Wang, N.; Quan, H.; Zhang, F.; Fan, J.; Feng, H.; Cheng, M.; Liao, Z.; Wang, X.; Xiang, Y. Yield and water productivity of crops, vegetables and fruits under subsurface drip irrigation: A global meta-analysis. *Agric. Water Manag.* **2022**, *269*, 107645. [CrossRef]
35. Gilbert, R.G.; Nakayama, F.S.; Bucks, D.A.; French, O.F.; Adamson, K.C.; Johnson, R.M. Trickle irrigation: Predominant bacteria in treated Colorado River water and biologically clogged emitters. *Irrig. Sci.* **1982**, *3*, 123–132. [CrossRef]
36. Nakayama, F.S.; Bucks, D.A. Water quality in drip/trickle irrigation: A review. *Irrig. Sci.* **1991**, *12*, 187–192. [CrossRef]
37. Yan, D.; Bai, Z.; Rowan, M.; Gu, L.; Ren, S.; Yang, P. Biofilm structure and its influence on clogging in drip irrigation emitters distributing reclaimed wastewater. *J. Environ. Sci.* **2009**, *21*, 834–841. [CrossRef] [PubMed]
38. Zhang, J.; Zhao, W.; Tang, Y.; Wei, Z.; Lu, B. Numerical investigation of the clogging mechanism in labyrinth channel of the emitter. *Int. J. Numer. Methods Eng.* **2007**, *70*, 1598–1612. [CrossRef]
39. Wei, Z.; Tang, Y.; Wen, J.; Lu, B. Two–phase flow analysis and experimental investigation of micro-PIV and anti-clogging for micro–channels of emitter. *Trans. Chin. Soc. Agric. Eng.* **2008**, *24*, 1–9.
40. Niu, W.; Yu, L.; Wu, P.; Fan, X.; Zhang, L. Influence of Angle of Labyrinth Channels on Anti-clogging Performance of Emitter. *Trans. Chin. Soc. Agric. Mach.* **2009**, *40*, 51–55.
41. Yu, L.; Wu, P.; Niu, W. Influence of the offset of labyrinth channels of drip emitters on hydraulic and anti-clogging performance. *Trans. Chin. Soc. Agric. Mach.* **2011**, *42*, 64–68.
42. Yu, L.; Tan, H.; Zou, X.; Chang, L.; Chen, L.; Fan, W. Numerical simulation of water and sediment flow in labyrinth channel based on coupled CFD-DEM. *Trans. Chin. Soc. Agric. Mach.* **2016**, *47*, 65–71. [CrossRef]
43. Yang, B.; Wang, J.; Zhang, Y.; Wang, H.; Ma, X.; Mo, Y. Anti-clogging performance optimization for dentiform labyrinth emitters. *Irrig. Sci.* **2020**, *38*, 275–285. [CrossRef]
44. Guo, S.; Zhang, C.; Guo, B.; Zhu, H.; Geng, W.; Chi, J. Influence of tooth width of single internal tooth emitter on its anti–clogging performance. *Water Sav. Irrig.* **2022**, *6*, 66–71.
45. Wang, X. Study on Anti–clogging Performance and Structural Parameters Optimization of Bidirectional Flow Channel Emitter in Drip Irrigation. Ph.D. Thesis, Xi'an University of Technology, Xi'an, China, 2019.
46. Yang, P.; Lei, X. Developments and study situations of drip irrigation emitters. *Water Sav. Irrig.* **2000**, *3*, 17–18.
47. Wang, X.; Yang, P.; Huang, L. Impact of fertilization and top-addressing on yield and quality of solar greenhouse cucumber under trae irrigation. *J. Irrig. Drain.* **2019**, *38*, 36–41. [CrossRef]
48. Chen, L.; Zheng, J.; Gao, J.; Miao, H. Generation of typhoon disaster emergency alternative based on fuzzy risk assessment. *J. Saf. Environ.* **2022**, *22*, 1467–1476. [CrossRef]
49. Wang, J.; Yang, X.; Jang, Y. Benefit Distribution Model of Military Supply Chain under the Background of Additive Manufacturing Technology. *J. Mil. Transp.* **2022**, *1*, 58–63.
50. Xu, X.; Yao, X. Research on Equipment Maintenance Strategy for Small and Medium Coal Mine Enterprises. *Coal Mine Mach.* **2022**, *43*, 173–178. [CrossRef]
51. Gilbert, R.G.; Nakayama, F.S.; Bucks, D.A.; French, O.F.; Adamson, K.C. Trickle irrigation: Emitter clogging and other flow problems. *Agric. Water Manag.* **1981**, *3*, 159–178. [CrossRef]
52. Kreij, C.; Burg, M.; Runia, T. Drip irrigation emitter clogging in Dutch greenhouses as affected by methane and organic acids. *Agric. Water Manag.* **2003**, *60*, 73–85. [CrossRef]

53. Wang, G.; Yang, F.; Wu, K.; Ma, Y.; Peng, C.; Liu, T.; Wang, L. Estimation of the dissipation rate of turbulent kinetic energy: A review. *Chem. Eng. Sci.* **2021**, *229*, 116133. [CrossRef]
54. Tang, X.; Zhao, X.; Li, Y.; Li, X. Numerical simulation of flow fields and particle movement characteristics in labyrinth channel emitter using different turbulence models. *Trans. Chin. Soc. Agric. Eng.* **2018**, *34*, 120–128.
55. Wang, F. *Computational Fluid Dynamics Analysis—CFD Software Principle and Application*; Tsinghua University Press: Beijing, China, 2004.
56. Chu, L.; Chen, W.; Li, X.; Liu, P. Researches on energy consumption mechanism and energy–saving principles of hydrocydones IV. The distribution and dissipation of turbulent kinetic energy. *Chem. Eng. Mach.* **1998**, *25*, 254–258.
57. Zhang, J. Evaluation of Hydraulic and Anti-clogging Performances and Structural Optimization of Labyrinth-Channel Emitters. Ph.D. Thesis, Xi'an Jiaotong University, Xi'an, China, 2009.
58. Zhang, J.; Zhao, W.; Tang, Y.; Lu, B. Anti–clogging performance evaluation and parameterized design of emitters with labyrinth channels. *Comput. Electron. Agric.* **2010**, *74*, 59–65. [CrossRef]
59. Bannayan, M.; Hoogenboom, G. Using pattern recognition for estimating cultivar coefficients of a crop simulation model. *Field Crop Res.* **2009**, *111*, 290–302. [CrossRef]
60. Dettori, M.; Cesaraccio, C.; Motroni, A.; Spano, D.; Duce, P. Using CERES-Wheat to simulate durum wheat production and phenology in Southern Sardinia, Italy. *Field Crop Res.* **2011**, *120*, 179–188. [CrossRef]
61. Zhuang, C.; He, C. *Fundamentals of Applied Mathematical Statistics*, 4th ed.; South China University of Technology Press: Guangzhou, China, 2013; p. 436.
62. Tian, J.; Bai, D.; Ren, C.; Wang, X. Analysis on hydraulic performance of bidirectional flow channel of drip irrigation emitter. *Trans. Chin. Soc. Agric. Eng.* **2013**, *29*, 89–94. [CrossRef]
63. Li, J.; Bai, D.; Wang, X.; Guo, L. Geometric parameters design and experimental study on new type drip emitter. *J. Drain. Irrig. Mach. Eng.* **2020**, *38*, 95–101. [CrossRef]
64. Xing, S.; Wang, Z.; Zhang, J.; Liu, N.; Zhou, B. Simulation and verification of hydraulic performance and energy dissipation mechanism of perforated drip irrigation emitters. *Water* **2021**, *13*, 171. [CrossRef]
65. Xu, T.; Zhang, L. Influence and analysis of structure design and optimization on the performance of a pit drip irrigation emitter. *J. Irrig. Drain.* **2020**, *69*, 633–645. [CrossRef]
66. Hu, Y.; Peng, J.; Yin, F.; Liu, X.; Li, N. Optimization of trapezoidal labyrinth emitter channel based on MATLAB and COMSOL co–simulation. *Trans. Chin. Soc. Agric. Eng.* **2020**, *36*, 158–164. [CrossRef]
67. Capra, A.; Scicolone, B. Water quality and distribution uniformity in drip/trickle irrigation systems. *J. Agric. Eng. Res.* **1998**, *70*, 355–365. [CrossRef]
68. Wang, X.; Li, J.; Shan, B.; Wang, G. Structural design and optimization of triangle circulation drip irrigation emitters. *Trans. Chin. Soc. Agric. Mach.* **2010**, *41*, 43–46. [CrossRef]
69. Sun, H.; Li, Y.; Ji, F.; Liu, H.; Liu, Y. Effects of flow path boundary optimizations on particle transport in drip irrigation emitters. *J. Irrig. Drain.* **2016**, *65*, 417–425. [CrossRef]
70. Wang, H.; Wang, J.; Wang, C.; Wang, S.; Qiu, X.; Sun, Y.; Li, G. Characterization of labyrinth emitter-clogging substances in biogas slurry drip irrigation systems. *Sci. Total Environ.* **2022**, *820*, 153315. [CrossRef] [PubMed]
71. Yuan, W.; Wei, Z.; Chu, H.; Ma, S. Optimal design and experiment for divided–flow emitter in drip irrigation. *Trans. Chin. Soc. Agric. Eng.* **2014**, *30*, 117–124. [CrossRef]
72. Wang, W.; Wang, F.; Niu, W.; Hu, X. Numerical analysis of influence of emitter channel structure on suspended granule distribution. *Trans. CSAE* **2009**, *25*, 1–6. [CrossRef]
73. Yu, L.; Yu, X.; Guo, H.; Wang, T.; Cui, N.; Li, N. Mechanism and anti–clogging of labyrinth–channel emitters under fluctuated water pressure. *Trans. Chin. Soc. Agric. Mach.* **2022**, *53*, 342–349. [CrossRef]
74. Chu, H.; Wei, Z.; Ma, S.; Yuan, W. Multi–objective optimization of Karman vortex street emitter based on grey relational analysis. *J. Irrig. Drain.* **2015**, *34*, 99–103. [CrossRef]
75. Özekici, B.; Sneed, R.E. Analysis of pressure losses in tortuous–path emitters. In *Paper–American Society of Agricultural Engineers (USA)*; American Society of Agricultural Engineers: St. Joseph, MI, USA, 1991; 19p.
76. Li, Y.; Yang, P.; Ren, S. General review on several fundamental points of design theory about flow path in drip irrigation emitters. *Trans. Chin. Soc. Agric. Mach.* **2006**, *37*, 145–148.

Disclaimer/Publisher's Note: The statements, opinions and data contained in all publications are solely those of the individual author(s) and contributor(s) and not of MDPI and/or the editor(s). MDPI and/or the editor(s) disclaim responsibility for any injury to people or property resulting from any ideas, methods, instructions or products referred to in the content.